JOURNAL OF CHEMICAL INFORMATION AND MODELING

Article

pubs.acs.org/jcim

Exploring the Desumoylation Process of SENP1: A Study Combined MD Simulations with QM/MM Calculations on SENP1-SUMO1-RanGAP1

Ting Shi,[†,∥] Yuhui Han,[†,∥] Weihua Li,[‡] Yanlong Zhao,[†] Yaqin Liu,[†] Zhimin Huang,[†] Shaoyong Lu,[†] and Jian Zhang*[,†]

[†]Department of Pathophysiology, Key Laboratory of Cell Differentiation and Apoptosis of Chinese Ministry of Education, Shanghai Jiao-Tong University School of Medicine, Shanghai 200025, China

[‡]Shanghai Key Laboratory of New Drug Design, School of Pharmacy, East China University of Science and Technology, Shanghai 200237, China

Supporting Information

ABSTRACT: The small ubiquitin-related modifier (SUMO)-specific protease (SENP) processes SUMOs to mature forms and deconjugates them from various modified substrates. Loss of the equilibrium from desumoylation catalyzed by abnormal SENP1 is associated with cancers and transcription factor activity. In spite of the significant role of SENP1, the molecular basis of its desumoylation remains unclear. Here, MD simulations and QM/MM methods are combined to investigate the catalytic mechanism of desumoylation. The results showed that substrate SUMO1-RanGAP1 fitted into the catalytic pocket of SENP1 by the break of internal hydrophobic interactions and the isomerization of isopeptide from *trans* to *cis*. After that, the nucleophilic sulfur anion of Cys603 in SENP1 attacked the carbonyl carbon of Gly97 of SUMO1 to trigger the reaction, and then a tetrahedral intermediate and an acyl-enzyme intermediate were generated in turn, leading to the final release of enzyme SENP1 and two products, free SUMO1 and RanGAP1. In the process, nucleophilic attack was identified as the rate-determining step with a potential energy barrier of 20.2 kcal/mol. These results are in agreement with experimental data from mutagenesis and other experiments. Our findings elucidate the catalytic mechanism of SENP1 with its substrate and may provide a better understanding of SENP desumoylation. In particular, we have identified key residues in SENP1 needed for desumoylation that might be beneficial for the design of novel inhibitors of SENP1-related diseases.

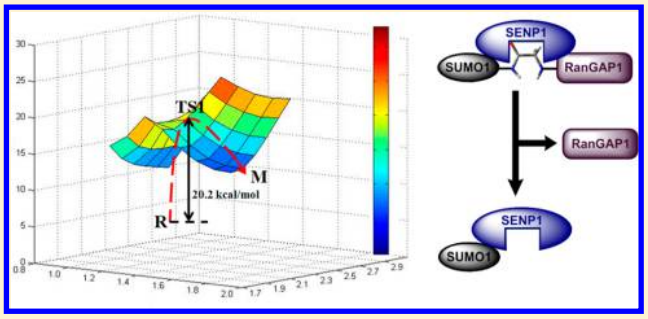

INTRODUCTION

Small ubiquitin-related modifier (SUMO) is a member of the ubiquitin-like protein family that modulates the cellular function of a variety of target proteins.[1−4] It has emerged as an important new post-translational modifier of proteins that can participate in transcriptional regulation, nuclear transport, maintenance of genome integrity, and signal transduction.[5,6] The dysfunction of SUMO modification is associated with a broad range of diseases, including cancers, neurodegenerative syndromes, diabetes, viral infections, and developmental defects.[7] Mammalian genomes contain four SUMO genes: SUMO1, SUMO2, SUMO3, and SUMO4.[8] All SUMO proteins are expressed as precursors, and SUMO-specific proteases (SENPs, also known as sentrin-specific proteases) catalyze the maturation process and expose the conserved C-terminal "GG" motif. Once mature SUMO proteins have been conjugated to a substrate either as a single entity or as a polymeric chain, SENP activity is required for chain depolymerization and deconjugation from substrates.[9]

Recently, interest has shifted to SENPs, which exhibit isopeptidase activity against a select subset of sumoylated substrates. In addition, eight human SENPs exhibit multiple splice variants that add to the functional diversity of the individual enzymes. Each of these proteins appears to have a distinct subcellular localization and substrate specificity during deconjugation.[10−13] Among them, SENP1 mainly localizes to foci in the nucleus and nuclear rim.[14,15] It processes SUMO-1 with greater efficiency than it processes SUMO-2 and SUMO-3, although the proteolysis of all SUMOs by SENP1 has been detected *in vitro*.[16] SENP1 deletion or inactivation in mice causes severe fetal anemia stemming from deficient erythropoietin production and death midgestation,[17,18] demonstrating its critical importance for regulating desumoylation in mammals. In addition, retroviral insertional mutation of SENP1 causes increased steady-state levels of the sumoylated forms of a number of proteins and results in placental abnormalities

Received: April 26, 2013
Published: August 10, 2013

dx.doi.org/10.1021/ci4002487 | *J. Chem. Inf. Model.* 2013, 53, 2360−2368

incompatible with embryonic development.[19] Notably, overexpression of SENP1 is closely associated with prostate cancer development[20−22] and thyroid oncocytic tumors.[23] Although physiological and biochemical studies have examined the function of SENP1, the molecular basis of the catalytic mechanism underlying SUMO regulation remains unclear.

To obtain a better insight into the desumoylation process catalyzed by SENP1, we combined molecular dynamic (MD) simulations with quantum mechanics/molecular mechanics (QM/MM) calculations on the SENP1-SUMO1-RanGAP1 system in an aqueous environment. In the study, we reported the conformational transitions of both SENP1 and SUMO1-RanGAP1 by induced-fit interactions for mutual recognition and catalytic preparation. QM/MM calculations were employed to investigate the detailed catalytic mechanism. Two-dimensional potential energy surfaces were obtained to locate the key intermediates and transition states. The desumoylation process was proposed, and the potential energy barriers were provided. These results are in good agreement with biochemical and structural studies. Our study elucidates the catalytic mechanism of SENP1 with its substrate, SUMO1-RanGAP1, provides a full insight into the desumoylation process of SENP1, and furthers the development of new therapeutic compounds for related diseases.

MATERIALS AND METHODS

System Preparation. Initial coordinates for free SENP1 and SUMO1-RanGAP1 and the SENP1-SUMO1-RanGAP1 complex were taken from the X-ray crystal structures (PDB entries: 2IY0 and 2IYC).[24] The functional Cys603 in SENP1 was retrieved from alanine, and the side chains with missing coordinates were reconstructed using the fragment library of the Biopolymer module in Sybyl version 6.8.[25] SUMO modification with an isopeptide bond between the C-terminal carboxyl group of Gly97 in SUMO1 and the ε-amino group of Lys524 in RanGAP1 was optimized at the level of HF/6-31G* using Gaussian 09,[26] and the parameters used in MD simulations were built in the xLeap module of the AMBER program suite.[27]

MD Simulations. The prepared structures mentioned above were taken as the starting points for MD simulations. Each MD simulation was carried out using the AMBER program suite with the Parm03 force field. Each structure was prepared with the xLeap module, in which protons were added to the structure. All ionizable side chains were maintained in their standard protonation states at pH 7.0. The proteins were solvated in a cubic box of TIP3P water molecules with a water thickness extending at least 10 Å away from the protein surface. Eight chloride ions as counterions were then added to the system to create a neutral simulation system.

To avoid any instability that might occur during the MD simulations, the solvated system was subjected to minimization for 5000 cycles with the proteins restrained and followed by another 5000 cycles with the whole system relaxed. Then, the system was gradually heated from 0 to 300 K during the first 60 ps in three intervals, followed by equilibrium for 80 ps under conditions of constant volume and temperature (NVT). Afterward, the system was switched to constant pressure and temperature (NPT) and equilibrated for 100 ps to adjust the system to the correct density. Finally, the production simulations were carried out in the absence of any restraint under NPT conditions, and 10-ns MD simulation was conducted. This protocol was applied to all of the simulation systems.

All MD simulations were performed using the parallel version of PMEMD in the AMBER suit. The Particle Mesh Ewald (PME) method[28] was employed to calculate long-range electrostatic interactions, and the lengths of bonds involving hydrogen atoms were fixed with the SHAKE algorithm.[29] During simulations, an integration time step of 2 fs was adopted, and structural snapshots were flushed every 500 steps (1 ps). The nonbonded cutoff was set to 10.0 Å, and the nonbonded pair list was updated every 25 steps. Each production simulation was coupled to a 300 K thermal bath at 1.0 atm by applying the Berendsen algorithm.[30] The temperature and pressure coupling constants were set to 2.0 and 1.0 ps, respectively.

Free Energy Calculation. Molecular mechanics Poisson−Boltzmann surface area (MM-PBSA) is a popular method for the computation of free energies that was first developed by Kollman et al. in 2000.[31,32] A number of successful applications of the MM-PBSA method have already been reported in the literature.[33−37] The MM-PBSA method implemented in the AMBER9 program was applied to compute the difference of the free energies (ΔG) in solution between *cis* and *trans* configurations of SUMO1-RanGAP1. The MM-PBSA method can be conceptually summarized as

$$\Delta G = G_{cis} - G_{trans} \tag{1}$$

$$G = E_{gas} + G_{sol} - TS \tag{2}$$

$$E_{gas} = E_{int} + E_{vdw} + E_{ele} \tag{3}$$

$$G_{sol} = G_{ele,sol} + G_{nonpol,sol} \tag{4}$$

$$G_{nonpol,sol} = \gamma \times SASA + b \tag{5}$$

Here, the comparison of the free energies (ΔG) is computed as the difference between the free energies of the *cis* SUMO1-RanGAP1 (G_{cis}) and the *trans* SUMO1-RanGAP1 (G_{trans}). The free energy of each molecule was calculated using eq 2 by summing its internal energy in the gas phase (E_{gas}), the solvation free energy (G_{sol}), and a vibrational entropy term (TS) computed by the Normal-Mode Analysis. E_{gas} is the standard force field energy, including strain energies from covalent bonds and torsion angles as well as noncovalent van der Waals and electrostatic energies (eq 3). The solvation free energy (G_{sol}) was computed as the sum of the electrostatic component and nonpolar component (eq 4). The electrostatic component was computed with the Possion-Boltzmann method (PB),[38] and the nonpolar component was assumed to be proportional to the solvent-accessible surface area ($SASA$) of the molecule under consideration. Because entropy calculation is extremely time-consuming for large systems and the contribution of entropy to ΔG may be negligible between the *trans* and *cis* configurations in SUMO1-RanGAP1,[39,40] the entropy term was not calculated in the MM-PBSA for the study.

QM/MM Calculation. QM/MM calculations were performed using a two-layered ONIOM method encoded in the Gaussian09 program. The ONIOM method[41−45] is a hybrid computational method developed by Morokuma and coworkers that allows different levels of theory to be applied to different parts of a molecular system.[46−48]

dx.doi.org/10.1021/ci4002487 | J. Chem. Inf. Model. 2013, 53, 2360−2368

The structure most similar to the average of the dominant cluster obtained with the AMBER Parm99 force field was further optimized at the ONIOM (B3LYP/6-31G*:Amber) level. The quantum mechanics (QM) region included the isopeptide bond between residues Gly97 in SUMO1 and Lys524 in RanGAP1, the methylenethioalcohol group ($-CH_2-S^{\gamma}H$) of Cys603, the terminal group ($-CH_2-CO^{\epsilon}N^{\zeta}H_2$) of Gln597, the anionic carboxymethyl group ($-CH_2-CO^{\delta1}O^{\delta2-}$) of Asp550, the side chain of His533, and a water molecule, for a total of 54 atoms. This brought the total charge of the QM system to −1 (the total system remained neutral). The QM region was calculated using the density functional theory with the B3LYP exchange-correlation functional and the 6-31G* basis set. The remainder of the system (MM region) was treated using the AMBER Parm99 force field. A total of 10,551 atoms were included in the QM/MM calculations. The electrostatic interactions between the QM and MM regions were calculated using the electronic embedding method, which treats the polarization of the QM region by the MM region with scaled partial atomic charges of MM atoms, and the response of the QM region with the Merz−Singh−Kollman scheme for charge fitting to produce the changing partial charges of the QM atoms. Furthermore, the PROPKA program[49] (http://propka.ki.ku.dk/), one of the most commonly used empirical pK_a predictors, was introduced to evaluate the protonated state of residues in the biological process of the desumoylation catalyzed by SENP1. The results showed that, after substrate binding, the pK_a of Asp550 decreases from 4.70 to 4.06, while the pK_a of Cys603 increases from 11.01 to 11.63, indicating that Asp550 acquires protons more easily, and Cys603 loses them more readily. Therefore, the proton transfer pathway at the beginning of the catalytic mechanism appeared to be functioning properly.

RESULTS AND DISCUSSION

The main goal of this study was to investigate the desumoylation process of SUMO1-RanGAP1 catalyzed by SENP1, which has been reported to be closely related to the conformational rearrangement between the enzyme and substrate. To this end, three systems for 10-ns MD simulations were conducted: (1) the free-state enzyme SENP1, (2) the free-state substrate SUMO1-RanGAP1, and (3) the complex of SENP1-SUMO1-RanGAP1. QM/MM calculations were further used to study the mechanism of desumoylation catalyzed by SENP1. Two potential energy surfaces were calculated to obtain pivotal intermediates and transition states as well as the potential energy barrieries.

Conformational Rearrangement of SENP1 in Desumoylation. The X-ray crystal structure of the SENP1-SUMO1-RanGAP1 complex showed a closed catalytic environment between the enzyme and its substrate, indicating that conformational rearrangement of SENP1 is a fundamental prerequisite for catalysis following the binding of the target substrate.[50−52] By comparing the residue trajectories of the active site between free SENP1 and SENP1 bound to SUMO1-RanGAP1 (Figure 1), two pairs of parallel residues, Trp465-Val532 and His529-Trp534, were found to adopt notable conformational changes. The indole of Trp465 in SENP1 flipped approximately 90 degrees to cover the Gly-Gly dipeptide of SUMO1, and it functioned as a "lid" for the precise recognition of substrate SUMO1-RanGAP1 in SENP1. In yeast, mutagenesis of the corresponding residue (Trp448A) in SENP1 homologue Ulp1 eliminated the binding of Ulp1 to SUMO homologue Smt3, which supports the role of Trp465 of SENP1 in the recognition of substrate.[53] Then, the parallel residue Val532 was released from its hydrophobic interaction with Trp465, and its two terminal methyl groups moved to the opposite side of the "channel". Meanwhile, the channel expanded at the bottom by disruption of the van der Waals interaction between Trp534 and its parallel residue, His529, leading to the complete insertion of SUMO1-RanGAP1. Mutagenesis of the corresponding residue (Trp515H) in Ulp1 decreased the binding of Ulp1 to Smt3, and the consistency between theoretical and experimental data provides an insight for the function of Trp534 in SENP1.[53] After the binding of substrate, the catalytic triad of SENP1 (Cys603, His533, and Asp550) gathered together in a subtle but significant conformational transition (Figure 1) that brings them into functional alignment and triggers the RanGAP1desumoylation process, in which Cys603 has been confirmed by the mutant experiments.[52,54]

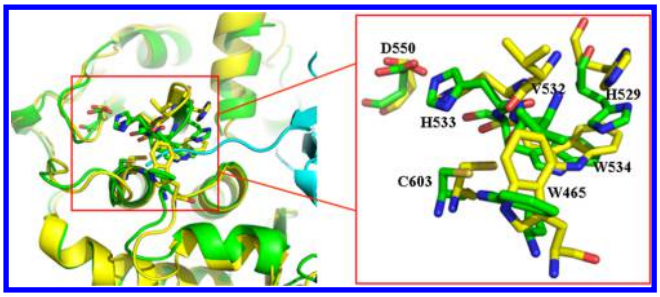

Figure 1. Comparison of SENP1 in free (green) and bound (yellow) states. The snapshot structures of SENP1 were extracted from the free SENP1 and SENP1-SUMO1-RanGAP1 trajectories at the time of 10 ns. The region of the catalytic channel in SENP1 is scaled up. SENP1 and SUMO1 (cyan in the system of SENP1-SUMO1-RanGAP1) are shown in a cartoon, and the side chains of crucial residues in SENP1 are depicted with sticks and labeled.

Conformational Transitions of SUMO1-RanGAP1. To further investigate the conformation transition of the SUMO1-RanGAP1 substrate, MD simulation was performed on free SUMO1-RanGAP1 (Figure S1). Compared with SENP1-SUMO1-RanGAP1, two important structural transformations in the free SUMO1-RanGAP1 were observed. First, the isomerization of the amide nitrogen from the *cis* to the *trans* configuration occurred in our simulation, although the X-ray crystal structure in the bound state indicates that the scissile isopeptide bond has the *cis* configuration (Figure 2).[24] As shown in Figure S2, this conformational transition was accomplished within 1 ns, and the isopeptide bond was found in the extended orientation and maintained the *trans* configuration after that. Second, another conformational transition induced by a hydrophobic interaction between residue Pro58 in SUMO1 and residues Leu560, Leu581, and Tyr585 in RanGAP1 was identified in the simulation. Specifically, Pro58 of SUMO1 gradually entered a hydrophobic pocket composed of the residues Leu560, Leu581, and Tyr585 of RanGAP1. This hydrophobic interaction emerged gradually in the initial 5 ns of the MD simulation and was stable in the following MD simulation. The root-mean-square fluctuation (RMSF) values of SUMO1 and RanGAP1 (Figure S3) also indicated that both SUMO1 and RanGAP1 residues close to the hydrophobic pocket have much larger fluctuations in the free state than in the bound state. Based on the analysis, we proposed that in addition to the conformational rearrange-

dx.doi.org/10.1021/ci4002487 | J. Chem. Inf. Model. 2013, 53, 2360−2368

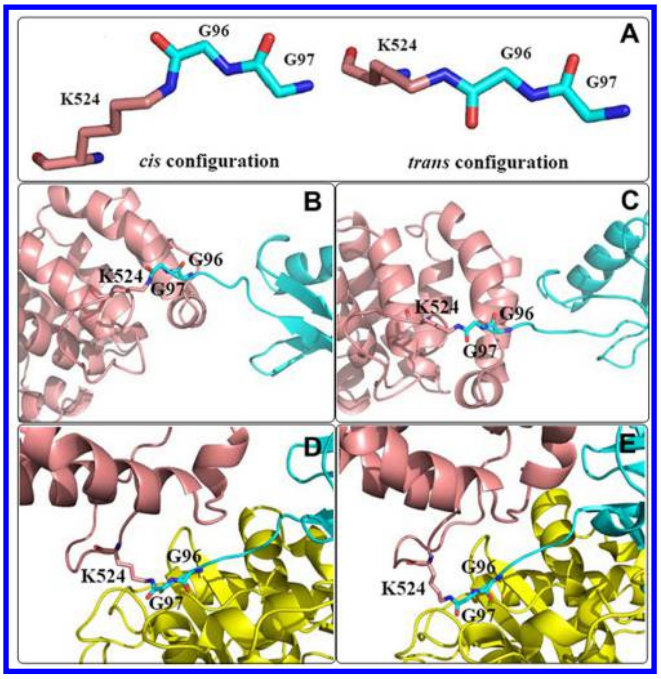

Figure 2. Isopeptide configurations of SUMO1-RanGAP1 in free and bound states with SENP1. **A**: The *cis* and *trans* configurations. **B**: The starting structure of SUMO1-RanGAP1. **C**: Snapshot of SUMO1-RanGAP1 at 10 ns. **D**: The starting structure of SENP1-SUMO1-RanGAP1. **E**: Snapshot of SENP1-SUMO1-RanGAP1 at 10 ns. SENP1 is shown in yellow, SUMO1 is shown in cyan, and RanGAP1 is shown in salmon.

ments of SENP1, SUMO1-RanGAP1 undergoes a large conformational change including the break of the hydrophobic patch between SUMO1 and RanGAP1, the isomerization of the isopeptide bond linking SUMO1 and RanGAP1, and the induced fit with the catalytic site of SENP1 during the binding process between SENP1 and SUMO1-RanGAP1. These results are in agreement with the fluorescence resonance energy transfer-based assay, which show that SENP1 binding is accompanied by a conformational change in the substrate.[24]

***Cis* Configuration of Isopeptide in SENP1-SUMO1-RanGAP1.** The configurations of the isopeptide might be *cis* or *trans* of the amino nitrogen under different environments[24,55−59] (Figure 2A). Our simulations demonstrated a stable *trans* arrangement for the isopeptide in the free state of SUMO1-RanGAP1. Furthermore, the total free energy obtained by the MM-PBSA method indicated that the *trans* arrangement is more favorable than the *cis* arrangement by 83.5 kcal/mol (Figure 2C and Table S1). However, when SUMO1-RanGAP1 was bound to SENP1, the *cis* arrangement of the isopeptide positioned the carbonyl carbon of Gly97 with respect to the sulfur of the active Cys603 such that nucleophilic attack can proceed (Figure 2E). Furthermore, two hydrogen bonds were formed between the carbonyl oxygen of Gly97 and the side chain NH of Gln597 and main chain NH of Cys603 in SENP1. Additionally, the NH groups in residues Gly97 and Lys524 formed hydrogen bonds with the carbonyl oxygen atom of Val532 (Figure 3A), and these hydrogen bonds were stable and permanent during the entire 10 ns simulation process (Table 1). Accordingly, we proposed that the *cis* configuration of the isopeptide might play a critical role in locking the position of the substrate, SUMO1-RanGAP1, in the active triad through hydrogen binding with residues Gln597, Cys603, and

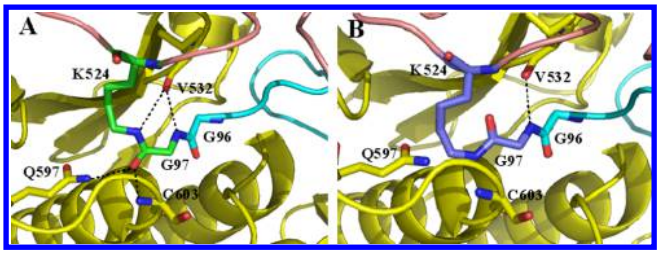

Figure 3. Key hydrogen bonds between the isopeptide and SENP1. **A**: *cis* configuration of the isopeptide in 10 ns snapshot of SENP1-SUMO1-RanGAP1 is shown in green. Hydrogen bonds are depicted by dashed lines. Colors for SENP1, SUMO1 and RanGAP1 are as in Figure 2. **B**: *trans* configuration of the isopeptide is shown in blue, and others are as in **A**.

Table 1. Hydrogen Bonds between the Isopeptide in SUMO1-RanGAP1 and SENP1 during 10 ns Simulations of the SENP1-SUMO1-RanGAP1 System

isopeptide in SUMO1-RanGAP1		SENP1			
residue	group	residue	group	distance (Å)[a]	occupancy (%)[b]
Gly97	O	Gln597	N^{ε}−H	2.925 (0.14)	98.39
Gly97	O	Cys603	N−H	3.187 (0.17)	78.89
Val532	O	Gly97	N−H	2.974 (0.14)	98.45
Val532	O	Lys524	N^{ζ}−H	3.012 (0.18)	88.06

[a]The average distance between hydrogen acceptor atom and hydrogen donor atom in the investigated time period. [b]Occupancy is hydrogen bond present percentage in the investigated time period.

Val532 for subsequent desumoylation. Notably, such anchor interactions were abolished when the isopeptide was in the *trans* conformation (Figure 3B, the *trans* structure was constrained to optimization). The mutational data revealed that Gln597A, which eliminated the hydrogen bond with the carbonyl oxygen of Gly97, is responsible for the correct orientation and leads to the severe impairment of both deconjugation and the processing activity of SENP1.[52]

Critical Role of Cysteine in the SENP1 Active Site. The structures of native SENP1 and its mutant Cys603S (PDB code is 2G4D) were carefully analyzed to understand the role of the cysteine in the active site (Figure 4). First, the orientations of

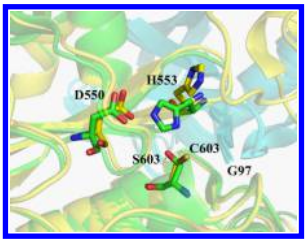

Figure 4. Comparison of the catalytic triad structures between SENP1 (PDB ID: 2IY0, carbon atoms from SENP1 are colored in yellow) and SENP1 Cys603S mutant (PDB ID: 2G4D, carbon atoms from SENP1 mutant are colored in green).

cysteine and serine in the catalytic triad were found to be different. The S^{γ} atom in Cys603 is directed at the carbonyl carbon of Gly97 in SUMO at a distance of 3.48 Å, whereas the O^{γ} atom in Ser603 is oriented to the $N^{\varepsilon 1}$ atom in His533 with 2.82 Å between them. In contrast, the distance between the O^{γ} atom and the reactive carbonyl carbon increases to 4.14 Å.

dx.doi.org/10.1021/ci4002487 | J. Chem. Inf. Model. 2013, 53, 2360−2368

Obviously, the orientation of S^{γ} atom is favorable for the desumoylation process, and this cysteine residue orientation is present in all known SENP crystal structures, including 2CKH,[60] 2IYD, 1TGZ,[50] and even the crystal structures of SENP8 with Neddylin.[60,61] Moreover, the $O^{\delta 1}$ atom in Asp550 participates in a strong hydrogen bond with the $N^{\varepsilon 2}$ atom in His553 at a distance of 2.84 Å, and the corresponding hydrogen bond distance for mutant Cys603S is 3.08 Å. This hydrogen bond induces a more electronegative imidazole group in His533, which cleaves the S^{γ}–H bond in Cys603, resulting in greater nucleophilicity for Cys603. Therefore, the orientation of the active cysteine and its microenvironment and the distances between the key residues are critical to SENP1 desumoylation activity, and the cysteine in SENP1 cannot be displaced by serine in its catalytic triad for SUMO1-RanGAP1. Mutagenesis experiments demonstrated that the lack of a thiol group in both Cys603S and Cys603A mutations inactivate the catalytic reaction in the desumoylation process.[52,54]

Catalytic Mechanism. To better understand the molecular basis of the catalytic mechanistic issues of SENP1, the equilibrated structure obtained with MD simulations in the SENP1-SUMO1-RanGAP1 system was further optimized at the ONIOM (B3LYP/6-31G*: Amber) level. A stable ground state structure **R** was located. Similar **R** ground states from other different conformations in the SENP1-SUMO1-RanGAP1 simulation were also observed after the ONIOM optimization (Figure S4), indicating that this state is a prerequisite for SENP1 catalytic mechanism. The major difference in **R** for the reaction center from the initial structure obtained by MD simulation was the identification of a proton transfer pathway from the thiol group of Cys603 to the carboxyl group of Asp550 through a water molecule and His533. Specifically, the hydrogen-bonded pairs include S^{γ}H–Cys603···O–Wat, OH–Wat···$N^{\varepsilon 1}$–His533, and $N^{\varepsilon 2}$H–His533···$O^{\delta 1}$–Asp550. This proton transfer pathway may contribute to the stability of the catalytic triad since the strong interactions between these hydrogen-bonded pairs lock the triad together. More importantly, the deprotonation of the thiol in Cys603, with high electronegativity, will facilitate nucleophilic attack on the carbonyl carbon of Gly97 in SUMO1. Taken together, these data suggest that the proton transfer pathway plays a critical role in the conformational rearrangement and desumoylation process.

A two-dimensional potential energy surface was calculated using the ONIOM (B3LYP/6-31G*:Amber) method to understand the nucleophilic attack of the electronegative S^{γ} atom of Cys603 on the carbonyl carbon of Gly97 in SUMO1. The potential energy surface was calculated by defining the distances of $r(S^{Cys603}–C^{Gly97})$ and $r(O^{Wat}–H^{Wat})$ as the reaction coordinates. The S^{Cys603}, C^{Gly97}, O^{Wat}, and H^{Wat} represent the S^{γ} atom of Cys603, the carbonyl carbon atom of Gly97, and the oxygen and hydrogen atoms of water, respectively. The potential energy surface with the key structures along the reaction path, including **R**, **TS1**, and **M**, is illustrated in Figure 5. The distance of $r(S^{Cys603}–C^{Gly97})$ was found to be 3.387 Å in the optimized structure **R** and 1.929 Å in the optimized product **M**, and the distance of $r(O^{Wat}–H^{Wat})$ is 1.006 Å in **R** and 1.691 Å in **M**. **TS1** is located at $r(S^{Cys603}–C^{Gly97})$ = 2.10 Å and $r(O^{Wat}–H^{Wat})$ = 1.30 Å. The nucleophilic attack was determined to be the rate-determining step with a calculated potential energy barrier of 20.2 kcal/mol, and we think the energy barrier might be even lower when different computational methods and/or indispensable solvent effects are considered. Besides, the tetrahedral intermediate **M** has been proposed by Shen et al.,[24] and the analogue is suggested by Berndsen et al.[62] in a mechanism involving direct nucleophilic attack of the N^{ζ}-Lysine on the enzyme-bound acetyl-CoA.

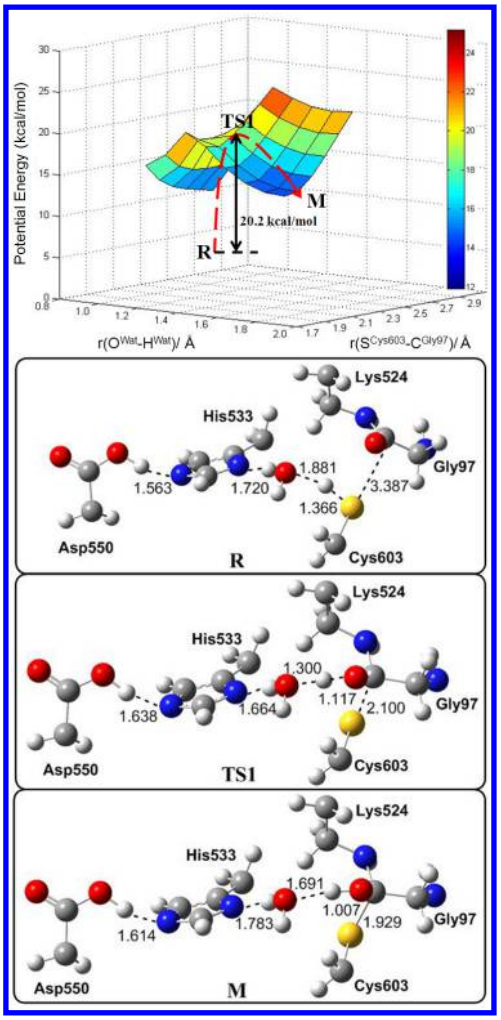

Figure 5. Two-dimensional potential energy surface defining the distances of $r(S^{Cys603}–C^{Gly97})$ and $r(O^{Wat}–H^{Wat})$ as the reaction coordinates and the key active-site structures of **R**, **M**, and **TS1** along the reaction path. Black dashed lines represent hydrogen bonds or key bond distances (in Å). For clarity, only the atoms around the reaction center are included. S^{Cys603}, C^{Gly97}, O^{Wat}, and H^{Wat} represent the S^{γ} atom of Cys603, the carbonyl carbon atom of G97, and the oxygen and hydrogen of water, respectively.

It should be noted that the proton transfer pathway was verified by **TS1**, which clearly demonstrated that the O^{Gly97}–H^{Wat} bond is almost formed (1.117 Å) and the O^{Wat}–H^{Wat} bond is almost broken (1.30 Å). The water entering into the active site may act not only as a proton transfer bridge but is also to stabilize **TS1.** To confirm our proposal, a catalytic pathway via a transition structure with the nucleophilic attack of the thiol group of Cys603 proceeding directly to the carbonyl carbon of Gly97 of SUMO1 was investigated. A calculated potential energy surface defining the distances of $r(S^{Cys603}–C^{Gly97})$ and $r(S^{Cys603}–H^{Cys603})$ as reaction coordinates was obtained. The transition state is located at $r(S^{Cys603}–C^{Gly97})$ = 2.00 Å and $r(S^{Cys603}–H^{Cys603})$ = 1.30 Å, and the potential energy barrier is calculated to be 40.2 kcal/mol (Figure S5). These computational results demonstrated that the activated

dx.doi.org/10.1021/ci4002487 | J. Chem. Inf. Model. 2013, 53, 2360–2368

energy barrier via a water-mediated **TS1** is 20.0 kcal/mol lower than without the proton transfer pathway.

Following the nucleophilic attack, the release of the target protein RanGAP1 was also investigated using a two-dimensional potential energy surface defining the distances of $r(N^{Lys524}–C^{Gly97})$ and $r(O^{Wat}–H^{Wat})$ as the reaction coordinates. The resulting two-dimensional potential energy surface is presented in Figure 6. The distance of $r(N^{Lys524}–C^{Gly97})$ was found to be 1.450 Å in the optimized structure **M** and increases to 3.316 Å in the optimized intermediate **M1**. The distance of $r(O^{Wat}–H^{Wat})$ is initially 1.007 Å in **M** and decreases to 2.097 Å in **M1**. Furthermore, **TS2** is located at $r(N^{Lys524}–C^{Gly97})$ = 1.60 Å and $r(O^{Wat}–H^{Wat})$ = 1.30 Å. In this reaction, proton transfer automatically proceeds from the carbonyl oxygen atom of Gly97 to a water molecule, followed by breaking of the $N^{Lys524}–C^{Gly97}$ bond as a result of the strong nucleophilic character of the Lys524 $N^{\zeta}H$. The hydrogen bond contributes to the near-attack reactive conformation, and the proton transfer is stabilized **TS2** through a water-mediated proton transfer pathway. In addition, the formation of the acyl-enzyme intermediate (SUMO1-SENP1) was found to be a rapid step, considering the activation barrier of 2.7 kcal/mol. Shen et al.[24] have suggested that the dissociation of the cleaved product is likely to be rapid, and our computational results are in good agreement with their analysis.

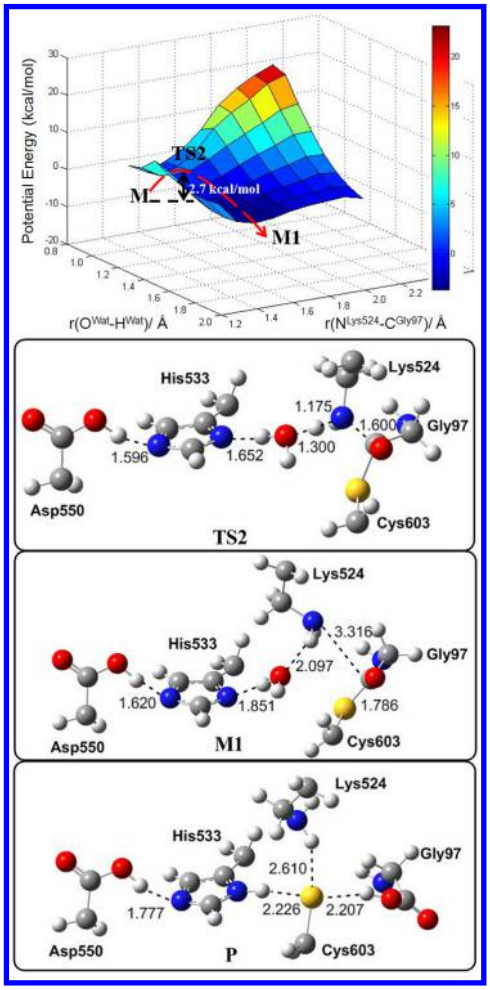

Figure 6. Two-dimensional potential energy surface defining the distances of $r(N^{Lys524}–C^{Gly97})$ and $r(O^{Wat}–H^{Wat})$ as the reaction coordinates and the key active-site structures of **TS2**, **M1**, and **P**. Black dashed lines represent hydrogen bonds or key bond distances (in Å). For clarity, only the atoms around the reaction center are included. N^{Lys524}, C^{Gly97}, O^{Wat}, and H^{Wat} represent the N^{ζ} atom of Lys524, the carbonyl carbon atom of G97, and the oxygen and hydrogen of water, respectively.

After the formation of the acyl-enzyme intermediate **M1**, hydrolysis occurs, and free SUMO1 and SENP1 are released in their *apo* forms and are then ready for the next reaction cycle. The structure of the hydrolysis product was designated as **P** (Figure 6). Compared with the stability of **M1** and **P**, we found that **M1** is less stable than **P** by 4.8 kcal/mol, suggesting that this hydrolysis process might proceed readily.

Taking these data together, we proposed a detailed reaction mechanism (Figure 7): (1) after the induced-fit mutual recognition between the enzyme (SENP1) and the substrate (SUMO1-RanGAP1), a proton transfers spontaneously from the $-S^{\gamma}H$ group of Cys603 to the carboxyl group of Asp550, and three hydrogen-bonded pairs are observed, including $S^{\gamma}H–Cys603\cdots O–Wat$, $OH–Wat\cdots N^{\varepsilon 1}–His553$, and $N^{\varepsilon 2}H–His553\cdots O^{\delta 1}–Asp550$; (2) the nucleophilic sulfur anion of Cys603 attacks the carbonyl carbon of Gly97 of SUMO1, leading to a tetrahedral intermediate **M**; (3) one product RanGAP1 is released from **M**; and (4) the acyl-enzyme intermediate **M1** is formed and then hydrolyzed to another product SUMO1 and enzyme SENP1. The mechanisms of enzymes on the isopeptides have been studied by several enzymes,[63−72] such as Ubiquitin C-terminal hydrolases (UCH-L1) and γ-Glutamyl hydrolase (GH). Generally, the hydrolysis mechanisms of these enzymes are performed as follows: (i) deprotonation of thiol group of cystine by adjacent basic histidine at the active site; (ii) nucleophilic attack of the deprotonated S^{-} on the carbonyl carbon of substrate; (iii) produce of thioester intermediate and release of amine segment from the substrate; (iv) hydrolysis of the thioester bond and release of the carboxylic segment from the substrate. In addition to the functions of cystine and histidine, aspartic acid of Cys-His-Asp generally enhances the basic property of histidine by forming a hydrogen bond for the following deprotonation of cystine. In SENP1, Asp550 participated in a strong hydrogen bond with His553 to induce more electronegative imidazole group of His533, which cleaved the $S^{\gamma}–H$ bond in Cys603, and the nucleophilic attack by the

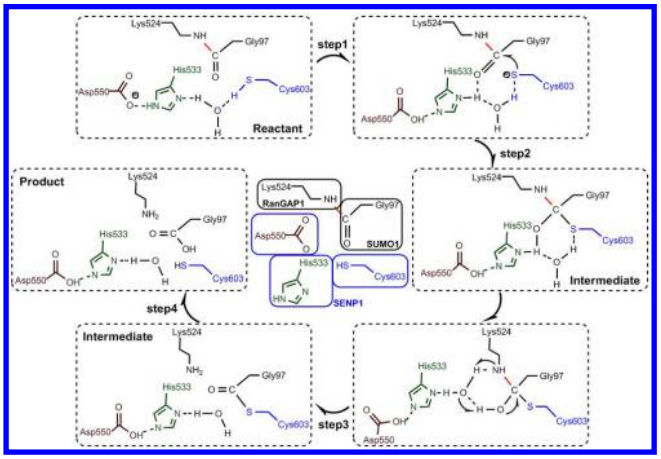

Figure 7. Catalytic reaction pathway obtained by QM/MM calculations. The isopeptide bond is shown in red, and the key residues in the triad are colored.

dx.doi.org/10.1021/ci4002487 | J. Chem. Inf. Model. 2013, 53, 2360−2368

deprotonated S^- of Cys603 on the carbonyl carbon of Gly97 of isopeptide lead to a tetrahedral intermediate. Finally, two products, RanGAP1 and SUMO1, were released. Basically, the mechanism of Cys603-His553-Asp550 is in agreement with the function of Cys-His-Asp found in UCH-L1 and GH. One water has been specifically found to be involved in proton transfers in the catalytic mechanism of SENP1, and to our knowledge, the hydrolysis energy on the isopeptide was first calculated in the study.

CONCLUSIONS

MD simulations and QM/MM calculations were conducted on the systems SENP1, SUMO1-RanGAP1, and SENP1-SUMO1-RanGAP1 to explore the desumoylation process and catalytic mechanism of SENP1 (Figure 8). In the process, substrate

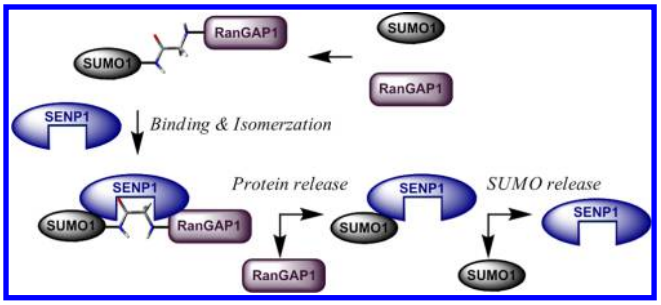

Figure 8. Proposed catalytic mechanism for the desumoylation of SUMO1-RanGAP1 by SENP1.

SUMO1-RanGAP1 breaks the hydrophobic patch between SUMO1 and RanGAP1, undergoes the isomerization of the isopeptide from *trans* to *cis*, and then embeds into the catalytic channel of enzyme SENP1 by induced-fit interactions. After that, the catalytic reaction of desumoylation is driven by SENP1 through two transition states. The nucleophilic sulfur anion of Cys603 attacks the carbonyl carbon of Gly97 of SUMO1 to form the first tetrahedral intermediate; after the release of free RanGAP1, the second acyl-enzyme intermediate is produced and hydrolyzed to free SUMO1 and SENP1. In the catalysis, the nucleophilic attack was identified to be the rate-determining step with a potential energy barrier of 20.2 kcal/mol. These findings are in good agreement with reported experimental and structural data and fully elucidate the desumoylation process of SENP1-SUMO1-RanGAP1 and further the discovery of compounds needed to treat related diseases.

ASSOCIATED CONTENT

Supporting Information

The RMSD values of SENP1, SUMO1-RanGAP1 and SENP1-SUMO1-RanGAP1 systems in 10 ns MD simulations (Figure S1) and the RMSF values of SUMO1 and RanGAP1 in the free state (SUMO1-RanGAP1) and the bound state (SENP1-SUMO1-RanGAP1) during 10 ns MD simulations (Figure S3). The conformational transition of the SUMO1-RanGAP1 system during its 10 ns MD simulation is shown in Figure S2. Comparison of the optimized arrangements of Cys603-His533-Asp550 in QM/MM from different conformations in the SENP1-SUMO1-RanGAP1 simulation is shown in Figure S4. A two-dimensional potential energy surface defined by the distances of $r(S^{Cys603}-C^{Gly97})$ and $r(S^{Cys603}-H^{Cys603})$ is shown in Figure S5. The free energies of SUMO1-RanGAP with the isopeptide in *cis* and *trans* configurations calculated by the MM-PBSA method are indicated in Table S1. This material is available free of charge via the Internet at http://pubs.acs.org.

AUTHOR INFORMATION

Corresponding Author

*Phone: +86-21-63846590-776922. Fax: +86-21-64154900. E-mail: jian.zhang@sjtu.edu.cn.

Author Contributions

‖T.S. and Y.H. contributed equally to this work.

Notes

The authors declare no competing financial interest.

ACKNOWLEDGMENTS

We would like to thank National Natural Science Foundation of China (21102090 and 81302698), the Shanghai Municipal Education Commission (13YZ032), the Shanghai Rising-Star Program (13QA1402300), the Program for New Century Excellent Talents in University (NCET-12-0355), the Program for Professor of Special Appointment (Eastern Scholar) at Shanghai Institutions of Higher Learning and the Shanghai PuJiang Program (10PJ406800), and the Ministry of Science and Technology of China (2009CB918404) for financial support of this work.

ABBREVIATIONS

SUMO, small ubiquitin-related modifier; SENP, SUMO-specific protease; MD, molecular dynamics; QM/MM, quantum mechanics/molecular mechanics; NVT, constant volume and temperature; NPT, constant pressure and temperature; PME, Particle Mesh Ewald; MM-PBSA, Molecular mechanics Poisson−Boltzmann; RMSF, root-mean-square fluctuation

REFERENCES

(1) Heun, P. SUMOrganization of the nucleus. *Curr. Opin. Cell Biol.* **2007**, *19*, 350−355.
(2) Martin, S.; Wilkinson, K. A.; Nishimune, A.; Henley, J. M. Emerging extranuclear roles of protein SUMOylation in neuronal function and dysfunction. *Nat. Rev. Neurosci.* **2007**, *8*, 948−959.
(3) Geiss-Friedlander, R.; Melchior, F. Concepts in sumoylation: a decade on. *Nat. Rev. Mol. Cell Biol.* **2007**, *8*, 947−956.
(4) Hay, R. T. SUMO: a history of modification. *Mol. Cell* **2005**, *18*, 1−12.
(5) Gareau, J. R.; Lima, C. D. The SUMO pathway: emerging mechanisms that shape specificity, conjugation and recognition. *Nat. Rev. Mol. Cel. Biol.* **2010**, *11*, 861−871.
(6) Zhao, J. Sumoylation regulates diverse biological processes. *Cell Mol. Life Sci.* **2007**, *64*, 3017−3033.
(7) Sarge, K. D.; Park-Sarge, O. K. SUMO and its role in human diseases. *Int. Rev. Cell Mol. Biol.* **2011**, *288*, 167−183.
(8) Owerbach, D.; McKay, E. M.; Yeh, E. T.; Gabbay, K. H.; Bohren, K. M. A proline-90 residue unique to SUMO-4 prevents maturation and sumoylation. *Biochem. Biophys. Res. Commun.* **2005**, *337*, 517−520.
(9) Hay, R. T. SUMO-specific proteases: a twist in the tail. *Trends Cell Biol.* **2007**, *17*, 370−376.
(10) Park, H. C.; Choi, W.; Park, H. J.; Cheong, M. S.; Koo, Y. D.; Shin, G.; Chung, W. S.; Kim, W. Y.; Kim, M. G.; Bressan, R. A.; Bohnert, H. J.; Lee, S. Y.; Yun, D. J. Identification and molecular properties of SUMO-binding proteins in Arabidopsis. *Mol. Cells* **2011**, *32*, 143−151.
(11) Nie, M.; Xie, Y.; Loo, J. A.; Courey, A. J. Genetic and proteomic evidence for roles of Drosophila SUMO in cell cycle control, Ras signaling, and early pattern formation. *PLoS One* **2009**, *4*, e5905.
(12) Mukhopadhyay, D.; Dasso, M. Modification in reverse: the SUMO proteases. *Trends Biochem. Sci.* **2007**, *32*, 286−295.

(13) Kim, J. H.; Baek, S. H. Emerging roles of desumoylating enzymes. *Biochim. Biophys. Acta* **2009**, *1792*, 155−162.
(14) Gong, L.; Millas, S.; Maul, G. G.; Yeh, E. T. Differential regulation of sentrinized proteins by a novel sentrin-specific protease. *J. Biol. Chem.* **2000**, *275*, 3355−3359.
(15) Bawa-Khalfe, T.; Cheng, J.; Wang, Z.; Yeh, E. T. Induction of the SUMO-specific protease 1 transcription by the androgen receptor in prostate cancer cells. *J. Biol. Chem.* **2007**, *282*, 37341−37349.
(16) Xu, Z.; Au, S. W. Mapping residues of SUMO precursors essential in differential maturation by SUMO-specific protease, SENP1. *Biochem. J.* **2005**, *386*, 325−330.
(17) Yu, L.; Ji, W.; Zhang, H.; Renda, M. J.; He, Y.; Lin, S.; Cheng, E. C.; Chen, H.; Krause, D. S.; Min, W. SENP1-mediated GATA1 deSUMOylation is critical for definitive erythropoiesis. *J. Exp. Med.* **2010**, *207*, 1183−1195.
(18) Cheng, J.; Kang, X.; Zhang, S.; Yeh, E. T. SUMO-specific protease 1 is essential for stabilization of HIF1alpha during hypoxia. *Cell* **2007**, *131*, 584−595.
(19) Yamaguchi, T.; Sharma, P.; Athanasiou, M.; Kumar, A.; Yamada, S.; Kuehn, M. R. Mutation of SENP1/SuPr-2 reveals an essential role for desumoylation in mouse development. *Mol. Cell. Biol.* **2005**, *25*, 5171−5182.
(20) Cheng, J.; Bawa, T.; Lee, P.; Gong, L.; Yeh, E. T. Role of desumoylation in the development of prostate cancer. *Neoplasia.* **2006**, *8*, 667−676.
(21) Bawa-Khalfe, T.; Cheng, J.; Lin, S. H.; Ittmann, M. M.; Yeh, E. T. SENP1 induces prostatic intraepithelial neoplasia through multiple mechanisms. *J. Biol. Chem.* **2010**, *285*, 25859−25866.
(22) Zuo, Y.; Cheng, J. K. Small ubiquitin-like modifier protein-specific protease 1 and prostate cancer. *Asian J. Androl.* **2009**, *11*, 36−38.
(23) Jacques, C.; Baris, O.; Prunier-Mirebeau, D.; Savagner, F.; Rodien, P.; Rohmer, V.; Franc, B.; Guyetant, S.; Malthiery, Y.; Reynier, P. Two-step differential expression analysis reveals a new set of genes involved in thyroid oncocytic tumors. *J. Clin. Endocrinol. Metab.* **2005**, *90*, 2314−2320.
(24) Shen, L.; Tatham, M. H.; Dong, C.; Zagorska, A.; Naismith, J. H.; Hay, R. T. SUMO protease SENP1 induces isomerization of the scissile peptide bond. *Nat. Struct. Mol. Biol.* **2006**, *13*, 1069−1077.
(25) *SYBYL*, Version 6.8; Tripos Associates Inc.: St. Louis, MO, 2001.
(26) Frisch, M. J.; Trucks, G. W.; Schlegel, H. B.; Scuseria, G. E.; Robb, M. A.; Cheeseman, J. R.; Montgomery, J. A., Jr.;Vreven, T.; Kudin, K. N.; Burant, J. C.; Millam, J. M.; Iyengar, S. S.; Tomasi, J.; Barone, V.; Mennucci, B.; Cossi, M.; Scalmani, G.; Rega, N.; Petersson, G. A.; Nakatsuji, H.; Hada, M.; Ehara, M.; Toyota, K.; Fukuda, R.; Hasegawa, J.; Ishida, M.; Nakajima, T.; Honda, Y.; Kitao, O.; Nakai, H.; Klene, M.; Li, X.; Knox, J. E.; Hratchian, H. P.; Cross, J. B.; Adamo, C.; Jaramillo, J.; Gomperts, R.; Stratmann, R. E.; Yazyev, O.; Austin, A. J.; Cammi, R.; Pomelli, C.; Ochterski, J. W.; Ayala, P. Y.; Morokuma, K.; Voth, G. A.; Salvador, P.; Dannenberg, J. J.; Zakrzewski, V. G.; Dapprich, S.; Daniels, A. D.; Strain, M. C.; Farkas, O.; Malick, D. K.; Rabuck, A. D.; Raghavachari, K.; Foresman, J. B.; Ortiz, J. V.; Cui, Q.; Baboul, A. G.; Clifford, S.; Cioslowski, J.; Stefanov, B. B.; Liu, G.; Liashenko, A.; Piskorz, P.; Komaromi, I.; Martin, R. L.; Fox, D. J.; Keith, T.; Al-Laham, M. A.; Peng, C. Y.; Nanayakkara, A.; Challacombe, M.; Gill, P. M. W.; Johnson, B.; Chen, W.; Wong, M. W.; Gonzalez, C.; Pople, J. A. *Gaussian09*, revision A.2; Gaussian, Inc.: Wallingford, CT, 2009.
(27) Case, D. A.; Darden, T. A.; Cheatham, T. E., III.; Simmerling, C. L.; Wang, J.; Duke, R. E.; Luo, R.; Walker, R. C.; Zhang, W.; Merz, K. M.; Roberts, B. P.; Wang, B.; Hayik, S.; Roitberg, A.; Seabra, G.; Kolossvary, I.; Wong, K. F.; Paesani, F.; Vanicek, J.; Liu, J.; Wu, X.; Brozell, S. R.; Steinbrecher, T.; Gohlke, H.; Cai, Q.; Ye, X.; Wang, J.; Hsieh, M. J.; Cui, G.; Roe, D. R.; Mathews, D. H.; Seetin, M. G.; Sagui, C.; Babin, V.; Luchko, T.; Gusarov, S.; Kovalenko, A.; Kollman, P. A. *AMBER 11*; University of California: San Francisco, 2010.
(28) Darden, T.; York, D.; Pedersen, L. Particle Mesh Ewald: an Nlog(N) method for Ewald sums in large systems. *J. Chem. Phys.* **1993**, *98*, 10089−10092.
(29) Ryckaert, J. P.; Ciccotti, G.; Berendsen, H. J. C. Numerical integration of the cartesian equations of motion of a system with constraints: molecular dynamics of n-alkanes. *J. Comput. Phys.* **1977**, *23*, 327−341.
(30) Berendsen, H. J. C.; Postma, J. P. M.; Van Gunsteren, W. F.; DiNola, A.; Haak, J. R. Molecular dynamics with coupling to an external bath. *J. Chem. Phys.* **1984**, *81*, 3684−3690.
(31) Massova, I.; Kollman, P. A. Combined molecular mechanical and continuum solvent approach (MM-PBSA/GBSA) to predict ligand binding. *Perspect. Drug Discovery Des.* **2000**, *18*, 113−135.
(32) Kollman, P. A.; Massova, I.; Reyes, C.; Kuhn, B.; Huo, S.; Chong, L.; Lee, M.; Lee, T.; Duan, Y.; Wang, W.; Donini, O.; Cieplak, P.; Srinivasan, J.; Case, D. A.; Cheatham, T. E. Calculating structures and free energies of complex molecules: combining molecular mechanics and continuum models. *Acc. Chem. Res.* **2000**, *33*, 889−897.
(33) Tzoupis, H.; Leonis, G.; Mavromoustakos, T.; Papadopoulos, M. G. A comparative molecular dynamics, MM−PBSA and thermodynamic integration study of saquinavir complexes with wild-type HIV-1 PR and L10I, G48V, L63P, A71V, G73S, V82A and I84V single mutants. *J. Chem. Theory Comput.* **2013**, *9*, 1754−1764.
(34) Martins, S. A.; Perez, M. A. S.; Moreira, I. S.; Sousa, S. F.; Ramos, M. J.; Fernandes, P. A. Computational alanine scanning mutagenesis: MM-PBSA vs TI. *J. Chem. Theory Comput.* **2013**, *9*, 1311−1319.
(35) Zhu, T.; Lee, H.; Lei, H.; Jones, C.; Patel, K.; Johnson, M. E.; Hevener, K. E. Fragment-based drug discovery using a multidomain, parallel MD-MM/PBSA screening protocol. *J. Chem. Inf. Model.* **2013**, *53*, 560−572.
(36) Srivastava, H. K.; Sastry, G. N. Molecular dynamics investigation on a series of HIV protease inhibitors: assessing the performance of MM-PBSA and MM-GBSA approaches. *J. Chem. Inf. Model.* **2012**, *52*, 3088−3098.
(37) Safi, M.; Lilien, R. H. Efficient a priori identification of drug resistant mutations using dead-end elimination and MM-PBSA. *J. Chem. Inf. Model.* **2012**, *52*, 1529−1541.
(38) Gilson, M. K.; Sharp, K. A.; Honig, B. H. Calculating the electrostatic potential of molecules in solution: method and error assessment. *J. Comput. Chem.* **1987**, *9*, 327−335.
(39) Zhou, Z.; Madrid, M.; Evanseck, J. D.; Madura, J. D. Effect of a bound non-nucleoside RT inhibitor on the dynamics of wild-type and mutant HIV-1 reverse transcriptase. *J. Am. Chem. Soc.* **2005**, *127*, 17253−17260.
(40) Zhao, Y.; Li, W.; Zeng, J.; Liu, G.; Tang, Y. Insights into the interactions between HIV-1 integrase and human LEDGF/p75 by molecular dynamics simulation and free energy calculation. *Proteins* **2008**, *72*, 635−645.
(41) Svensson, M.; Humbel, S.; Froese, R. D. J.; Matsubara, T.; Sieber, S.; Morokuma, K. ONIOM: a multilayered integrated MO + MM method for geometry optimizations and single point energy predictions. A test for Diels−Alder reactions and Pt(P(t-Bu)3)2 + H2 oxidative addition. *J. Phys. Chem.* **1996**, *100*, 19357−19363.
(42) Svensson, M.; Humbel, S.; Morokuma, K. Energetics using the single point IMOMO (integrated molecular orbital+molecular orbital) calculations: choices of computational levels and model system. *J. Chem. Phys.* **1996**, *105*, 3654−3661.
(43) Kuno, M.; Hannongbua, S.; Morokuma, K. Theoretical investigation on nevirapine and HIV-1 reverse transcriptase binding site interaction, based on ONIOM method. *Chem. Phys. Lett.* **2003**, *380*, 456−463.
(44) Vreven, T.; Byun, K. S.; Komaromi, I.; Dapprich, S.; Montgomery, J. A., Jr; Morokuma, K.; Frisch, M. J. Combining quantum mechanics methods with molecular mechanics methods in ONIOM. *J. Chem. Theory Comput.* **2006**, *2*, 815−826.
(45) Vreven, T.; Frisch, M. J.; Kudin, K. N.; Schlegel, H. B.; Morokuma, K. Geometry optimization with QM/MM Methods. II. Explicit Quadratic Coupling. *Mol. Phys.* **2006**, *104*, 701−714.

(46) Zhang, J.; Li, C.; Shi, T.; Chen, K.; Shen, X.; Jiang, H. Lys169 of human glucokinase is a determinant for glucose phosphorylation: implication for the atomic mechanism of glucokinase catalysis. *PLoS One* **2009**, *4*, e6304.
(47) Shi, T.; Lu, Y.; Liu, X.; Chen, Y.; Jiang, H.; Zhang, J. Mechanism for the autophosphorylation of CheA histidine kinase: QM/MM calculations. *J. Phys. Chem. B* **2011**, *115*, 11895−11901.
(48) Lu, S.; Huang, W.; Li, X.; Huang, Z.; Liu, X.; Chen, Y.; Shi, T.; Zhang, J. Insights into the role of magnesium triad in myo-inositol monophosphatase: metal mechanism, substrate binding, and lithium therapy. *J. Chem. Inf. Model.* **2012**, *52*, 2398−2409.
(49) Olsson, M. H. M.; Søndergaard, C. R.; Rostkowski, M.; Jensen, J. H. PROPKA3: consistent treatment of internal and surface residues in empirical pKa predictions. *J. Chem. Theory Comput.* **2011**, *7*, 525−537.
(50) Reverter, D.; Lima, C. D. A basis for SUMO protease specificity provided by analysis of human Senp2 and a Senp2-SUMO complex. *Structure* **2004**, *12*, 1519−1531.
(51) Xu, Z.; Chau, S. F.; Lam, K. H.; Chan, H. Y.; Ng, T. B.; Au, S. W. Crystal structure of the SENP1 mutant C603S-SUMO complex reveals the hydrolytic mechanism of SUMO-specific protease. *Biochem. J.* **2006**, *398*, 345−352.
(52) Shen, L. N.; Dong, C.; Liu, H.; Naismith, J. H.; Hay, R. T. The structure of SENP1-SUMO-2 complex suggests a structural basis for discrimination between SUMO paralogues during processing. *Biochem. J.* **2006**, *397*, 279−288.
(53) Mossessova, E.; Lima, C. D. Ulp1-SUMO crystal structure and genetic analysis reveal conserved interactions and a regulatory element essential for cell growth in yeast. *Mol. Cell* **2000**, *5*, 865−876.
(54) Bailey, D.; O'Hare, P. Characterization of the localization and proteolytic activity of the SUMO-specific protease, SENP1. *J. Biol. Chem.* **2004**, *279*, 692−703.
(55) Liu, Z.; Shang, Y.; Feng, J.; Peng, C.; Liu, H.; Hu, Y. Effect of hydrophilicity or hydrophobicity of polyelectrolyte on the interaction between polyelectrolyte and surfactants: molecular dynamics simulations. *J. Phys. Chem. B* **2012**, *116*, 5516−5526.
(56) Kang, S.; Huynh, T.; Xia, Z.; Zhang, Y.; Fang, H.; Wei, G.; Zhou, R. Hydrophobic interaction drives surface-assisted epitaxial assembly of amyloid-like peptides. *J. Am. Chem. Soc.* **2013**, *135*, 3150−3157.
(57) Niels, J. C.; Kasper, P. K. Accurate stabilities of laccase mutants predicted with a modified FoldX protocol. *J. Chem. Inf. Model.* **2012**, *52*, 3028−3042.
(58) Reverter, D.; Lima, C. D. Structural basis for SENP2 protease interactions with SUMO precursors and conjugated substrates. *Nat. Struct. Mol. Biol.* **2006**, *13*, 1060−1068.
(59) Huang, D. T.; Schulman, B. A. Breaking up with a kinky SUMO. *Nat. Struct. Mol. Biol.* **2006**, *13*, 1045−1047.
(60) Reverter, D.; Wu, K.; Erdene, T. G.; Pan, Z. Q.; Wilkinson, K. D.; Lima, C. D. Structure of a complex between Nedd8 and the Ulp/Senp protease family member Den1. *J. Mol. Biol.* **2005**, *345*, 141−151.
(61) Shen, L. N.; Liu, H.; Dong, C.; Xirodimas, D.; Naismith, J. H.; Hay, R. T. Structural basis of NEDD8 ubiquitin discrimination by the deNEDDylating enzyme NEDP1. *EMBO J.* **2005**, *24*, 1341−1351.
(62) Berndsen, C. E.; Albaugh, B. N.; Tan, S.; Denu, J. M. Catalytic mechanism of a MYST family histone acetyltransferase. *Biochemistry* **2007**, *46*, 623−629.
(63) Tan, L.; Li, M.; Turnbough, C. L., Jr. An unusual mechanism of isopeptide bond formation attaches the collagenlike glycoprotein BclA to the exosporium of Bacillus anthracis. *mBio* **2011**, *2*, e00084−11.
(64) Hu, X.; Hu, H.; Melvin, J. A.; Clancy, K. W.; McCafferty, D. G.; Yang, W. Autocatalytic intramolecular isopeptide bond formation in gram-positive bacterial pili: a QM/MM simulation. *J. Am. Chem. Soc.* **2011**, *133*, 478−485.
(65) Monbaliu, J. M.; Dive, G.; Stevens, C. V.; Katritzky, A. R. Governing parameters of long-range intramolecular S-to-N acyl transfers within (S)-acyl isopeptides. *J. Chem. Theory Comput.* **2013**, *9*, 927−934.
(66) Ferguson, A. L.; Zhang, S.; Dikiy, I.; Panagiotopoulos, A. Z.; Debenedetti, P. G.; James, L. A. An experimental and computational investigation of spontaneous lasso formation in microcin J25. *Biophys. J.* **2010**, *99*, 3056−3065.
(67) Alexander, J. P.; Ryan, T. J.; Ballou, D. P.; Coward, J. K. γ-Glutamyl hydrolase: kinetic characterization of isopeptide hydrolysis using fluorogenic substrates. *Biochemistry* **2008**, *47*, 1228−1239.
(68) Wang, H.; Vath, G. M.; Gleason, K. J.; Hanna, P. E.; Wagner, C. R. Probing the mechanism of hamster arylamine N-acetyltransferase 2 acetylation by active site modification, site-directed mutagenesis, and pre-steady state and steady state kinetic studies. *Biochemistry* **2004**, *43*, 8234−8246.
(69) Huang, Z.; Zhu, L.; Cao, Y.; Wu, G.; Liu, X.; Chen, Y.; Wang, Q.; Shi, T.; Zhao, Y.; Wang, Y.; Li, W.; Li, Y.; Chen, H.; Chen, G.; Zhang, J. ASD: a comprehensive database of allosteric proteins and modulators. *Nucleic Acids Res.* **2011**, *39*, D663−669.
(70) Liu, X.; Su, X.; Wang, F.; Huang, Z.; Wang, Q.; Li, Z.; Zhang, R.; Wu, L.; Pan, Y.; Chen, Y.; Zhuang, H.; Chen, G.; Shi, T.; Zhang, J. ODORactor: a web server for deciphering olfactory coding. *Bioinformatics* **2011**, *27*, 2302−2303.
(71) Kitadokoro, K.; Kamitani, S.; Miyazawa, M.; Hanajima-Ozawa, M.; Fukui, A.; Miyake, M.; Horiguchi, Y. Crystal structures reveal a thiol protease-like catalytic triad in the C-terminal region of Pasteurella multocida toxin. *Proc. Natl. Acad. Sci.* **2007**, *104*, 5139−5144.
(72) Das, C.; Hoang, Q. Q.; Kreinbring, C. A.; Luchansky, S. J.; Meray, R. K.; Ray, S. S.; Lansbury, P. T.; Ringe, D.; Petsko, G. A. Structural basis for conformational plasticity of the Parkinson's disease-associated ubiquitin hydrolase UCH-L1. *Proc. Natl. Acad. Sci.* **2006**, *103*, 4675−4680.